scientific reports

Check for updates

OPEN

Hydrogen sulfide preserves intestinal barrier repair function through sulfhydration of RPS20 in experimental colitis

Xuan He[1,5], Jichang Li[1,5], Zhihao Huang[2,5], Baoshuai Xue[3], Jing Zhu[1], Meiyi You[1], Xiaoyun Liu[4], Xin Wang[1], Yucun Liu[1], Shanwen Chen[1]✉ & Pengyuan Wang[1]✉

Patients with ulcerative colitis (UC) have a significantly impaired intestinal barrier. Hydrogen Sulfide (H_2S) is a gaseous mediator that makes notable contributions in a variety of diseases, such as reducing inflammatory response in colitis. The experimental content includes the establishment of a mouse DSS-induced colitis mouse model, mouse colon epithelial organoids culture, H&E staining and mass spectrometry analysis. We recognized that exogenous H_2S donor-GYY4137 significantly alleviated the symptoms in UC mice models and maintained Minichromosome Maintenance Complex Component 2 (MCM2) expression. CBS knockdown reduced the expression of sulfhydrated Ribosomal protein S20 (RPS20-ssh) and MCM2 in the mouse colon. Cell experiments indicated that the expression of RPS20-ssh, rather than total expression of RPS20, is responsible.

Our investigation indicated that CBS-H_2S axis increases the sulfhydration level of RPS20, leading to enhanced binding between RPS20 and MCM2 mRNA, thereby promoting intestinal epithelial proliferation. This may provide a novel therapeutic strategy for the clinical treatment of colitis.

Keywords H_2S, Intestinal barrier, IBD, Ulcerative colitis, MCM2

Abbreviations

H_2S	Hydrogen sulfide
UC	Ulcerative colitis
MCM2	Minichromosome maintenance complex component 2
RPS20	Ribosomal protein S20
HuR	Human antigen R
CBS	Cystathionine β-synthase
CSE	Cystathionine γ-lyase
3-MST	3-mercaptopyruvate sulfotransferase
IBD	Inflammatory bowel disease
RBP	RNA-binding protein
WT	Wild-type
DSS	Dextran sulfate sodium salt

The intestinal barrier plays a crucial role in separating the intestinal lumen from the internal milieu, thereby maintaining maintains mucosal homeostasis and immune balance[1,2]. The intestinal barrier is composed of three interdependent layers, comprising the luminal mucus layer, the intestinal epithelial layer, and the mucosal immune system[3]. During the development of colitis, the intestinal barrier undergoes damage, resulting in significantly increased intestinal permeability[4]. Therefore, the exploration of protective agents targeting intestinal barrier dysfunction may offer innovative therapeutic strategies for colitis.

Similar to nitric oxide and carbon monoxide, H_2S is a gaseous signaling molecule in the human body, primarily synthesized during cysteine metabolism and excreted by the kidneys as urinary sulfates[5,6]. Endogenous

[1]Department of Gastrointestinal Surgery, Peking University First Hospital, Beijing, China. [2]AstraZeneca Investment (China) Co., Ltd., Shanghai, China. [3]Key Laboratory of Zoonosis, Ministry of Education, College of Veterinary Medicine, Jilin University, Changchun, China. [4]School of Basic Medicine, Peking University, Peking University, Beijing, China. [5]Xuan He, Jichang Li and Zhihao Huang contributed equally to this work. ✉email: shanwen@pku.edu.cn; wangpengyuan2014@126.com

H_2S is mainly produced by the conversion of cysteine by Cystathionine β-synthase (CBS), cystathionine γ-lyase (CSE) and 3-mercaptopyruvate sulfotransferase (3-MST), while CBS is significantly reduced in intestinal tissues of human ulcerative colitis[7,8]. H_2S exerts protective effects in a variety of diseases, including but not limited to gastrointestinal disorders, cardiovascular diseases, and neurological disorders[8–11]. H_2S preserves endothelial cell functionality and retards the progression of atherosclerosis through sulfhydrating RNA-binding protein Human Antigen R (HuR)[11]. In gastrointestinal tissues, H_2S exhibits antioxidant properties, with glutathione playing a pivotal role in cellular ROS clearance. Research indicates that H_2S can elevate glutathione levels in the gastric mucosa, thus effectively reducing ROS levels[12]. Cumulative studies, including our prior researches, have demonstrated an association between diminished synthesis of H_2S primarily from CBS and various gastrointestinal diseases, such as UC[8,10]. Additionally, the beneficial effects of H_2S on intestinal barrier function have been linked to the inhibition of NLRP-3 inflammasome activation and NF-kB-mediated MLCK signaling[8]. GYY4137 is a novel, water-soluble exogenous H_2S-releasing molecule with anti-inflammatory activity and has been widely used in H_2S research[13]. However, in addition to its anti-inflammatory effects, whether H_2S contributes to maintaining intestinal epithelial repair function hence protecting the intestinal barrier in colitis remains to be illustrated.

MCM2 plays a critical role in cell proliferation, cell cycle regulation, DNA damage repair, and drug resistance[14]. In hepatocellular carcinoma (HCC) cells, MCM2 promotes stemness properties by modulating the Hippo signaling pathway, while its downregulation reduces sorafenib resistance[15,16]. At the same time, MCM2 can cooperate with ESRG to inhibit the p53 pathway, thereby supporting cell survival and self-renewal, or pluripotency of pluripotent stem cells[17]. MCM2 expression is regulated by multiple factors. Given that MCM2 serves as a determinant factor in cell proliferation ability, and considering the significantly reduced CBS expression in UC colon tissue[8], we hypothesized that the CBS-H_2S axis could regulate MCM2 expression, thereby modulating cell proliferation in the intestinal epithelium and promoting the repair of damaged intestinal tissue.

In this study, a 3.5% DSS solution was used to induce an experimental model of UC in mice. Compared with wild-type (WT) mice, CBS +/− heterozygous mice exhibited more severe colitis, increased intestinal permeability, and a significant reduction in intestinal epithelial repair function. The sulfhydration level of RPS20 was found to be decreased in CBS +/− mice, accompanied by a reduction in MCM2 expression. To investigate the mechanism of H_2S regulating MCM2 expression, we conducted in vitro experiments using Caco-2 cells. After knocking out CBS, we observed decreases in cell proliferation ability, MCM2 expression level, and, significantly, the sulfhydration level of RPS20.

In summary, our results indicated that endogenous H_2S, primarily derived from CBS, plays a crucial role in preserving the integrity of intestinal barrier function and facilitating post-injury repair of intestinal epithelium in UC. The maintenance of RPS20-MCM2 axis might be the potential molecular mechanism, by which H_2S maintains cell proliferation in intestinal epithelium and other tissues.

Materials and methods

Mice

C57BL/6N wild-type (WT) mice were bred in the Animal Center of Peking University First Hospital. The mouse CBS gene (GenBank accession number: NM_144855.3; Ensembl: ENSMUSG00000024039) is located on mouse chromosome 17, and exon 3 to exon 14 was selected as target site for knockout. Cas9 mRNA and gRNA generated by in vitro transcription were injected into fertilized eggs to produce knockout mice. All mouse experiments were approved by the Animal Ethics Committee of Peking University First Hospital (No. J2022082) and we confirmed the study is reported in accordance with ARRIVE guidelines (https://arriveguidelines.org). Genotype identification was performed by PCR using tail genomic DNA, and the primer sequences were as follows: mouse CBS-F: 5'-AGGGAGAAGTTACATCATGCCTTGG-3', mouse CBS-R: 5'-AGTATCCAGGGCTTGACATCCTTA-3', and mouse CBS-WT/He-F: 5'-CTGATGCGGTTTCCTAGCAACAG-3'. The size of the PCR products was 1,055 bp for WT mice, and 1,055 bp and 810 bp for CBS +/− mice (Fig. S1A). All CBS + /- male mice were fed for 6 weeks after birth.

Animal Treatment

The ulcerative colitis mice model was induced by voluntary ingestion of 3.5% DSS in water (PM, America). 30 WT and 30 CBS + /- mice were randomly grouped into Control, DSS and DSS + GYY4137(a novel water-soluble, H_2S-releasing molecule). Our previous experiments and a large number of literatures showed that 500 μg/10 g/day GYY4137 had a significant anti-inflammatory effect, so we chose 500 μg/10 g/day GYY4137 as the experimental concentration[10,13,18]. Control mice were treated with water at baseline and injected intraperitoneally with 100 μl/10 g PBS every day from day 1 to 7. Mice in the DSS group were injected intraperitoneally with 100 μl/10 g PBS every day from day 1 to 7, and orally administered 3.5% DSS every day from day 0 to 7. Mice in the DSS + GYY4137 group were injected with 500 μg/10 g GYY4137 (Sigma Aldrich, America) in PBS every day from day 1 to 7, and orally administered 3.5% DSS every day from day 0 to 7. After 7 days of treatment, all mice were euthanized with intraperitoneal injection of pentobarbital sodium (200 mg/kg).

Using the same treatment method, mice were served with normal water from the eighth day, until being euthanized after 21 days of treatment.

DAI score evaluation

Disease activity index (DAI) scoring system was used to assess the clinical conditions of mice in each group (10 per group), and the scoring method is shown in Table 1. Three independent researchers performed blind scoring work including weight loss, stool consistency and fecal occult blood[19].

DAI score of colon			
Score	Weight loss %	Stool consistency	Stool occult blood
0	0	Normal	Normal
1	1–5	Soft stool	Light blue stool
2	5–10	Mucoid stool	Blue poop
3	10–20	Thin liquid stool	Dark blue feces
4	> 20		Naked bloody stool

Table 1. The Disease activity index (DAI) of mice was assessed based on weight loss%, stool consistency, and stool occult blood.

Paracellular permeability detection of mice intestine

Mice intestinal permeability was detected as mentioned previously[20]. On the seventh day of the animal experiment, FD-4 (150 g/L, Sigma, America) was administered to mice by gavage at a dose of 40 µl/10 g body weight. 4 h after FD-4 gavage, we collected the blood samples and detected the serum fluorescence level using Synergy H2 microplate reader (Biotek Instruments, America) with 492 nm excitation and 520 nm emission filter.

Histological assessment of colon epithelium

The proximal colons of all groups of mice in day 7 and day 21 were excised and embedded with paraffin. Sections and hematoxylin and eosin (H&E) stain were performed on day 7. Images were obtained, at least six imaged per slide, using Zeiss imaging optical microscopes with magnifications of 40x, 100x, and 400x. The extent of histopathological alterations was assessed by three pathologists who were unaware of grouping and grading based on the scoring method previously mentioned. Sections were graded according to inflammation severity, degree, crypt damage scores were calculated by multiplying the scores of each sections by their percentage of involvement, with a minimum score of 0 and a maximum score of 40: cellular infiltration (0–5), deterioration of crypt structure (crypt damage, 0–4), degree of mucosal ulceration (0–3), and presence of submucosal edema (0 and 1)[21]. Three doctors who were blinded to the groups were selected and histopathological scores were assessed by three clinical doctors. Masson staining was performed on tissues after 21 days, followed by measuring the thickness of fibrosis[22].

Organoid culture

For isolation and establishment of primary colon organoids, colon was minced and incubated in DMEM-F12 Advance (Thermo, America), 5 mg/mL Collagenase II, 1.25 mg/mL Dispase, 2.5% FBS, 100 × HEPES Buffer (Thermo, America), 100 × Glutamax (Thermo, America) and 100 ng/mL Primocin (Invivogen, America) on a rocker (Miltenyi, America) at 37 °C for 2–3 h. The sample was collected in DMEM-F12 Advance, 10% FBS, 100 × HEPES Buffer, 100 × Glutamax and 100 ng/mL Primocin, passed through a cell strainer filter and centrifuged at 850 rpm for 7 min at 4 °C. Then, 10 µL of 10 mg/mL DNase I were added and incubated at 37 °C for 5 min. Finally, the sample was resuspended in 100% Matrigel (8 mg/mL, Corning), plated in a pre-warmed 24-wells plate, and placed in the incubator at 37 °C for 30 min. When the Matrigel solidified, 500 µL of Complete Feeding Medium (Advanced DMEM-F12, 100xHEPES Buffer, 100 × Glutamax, 100 ng Primocin, 20% R-Spondin conditioned medium, 500 nM A83-01 (Sigma, America), 50 ng/mL hEGF (Preprotech), 100 ng/mL mNoggin (Preprotech), 100 ng/mL hFGF10 (Preprotech), 10 nM Gastrin I (TOCRIS), 3 µM SB202190 (Stem cell, America), 10 nM Prostaglandin E2 (TOCRIS), 1.25 mM N-acetylcysteine (Sigma, America), 10 mM Nicotinammide (Sigma), 1X B-27 Supplement (Thermo)) supplemented with 10.5 mM Y-27632 (Rho Kinase inhibitor) was added to the top of the Matrigel and the 24 well-plates placed in the incubator.

To split the primary colon organoids, droplets were broken by adding 1 mL of ice-cold Splitting Media (Advanced DMEM-F12, 100 × HEPES Buffer, 100 × Glutamax, 100 ng/mL Primocin) and pipetting up and down. Organoids were collected in a tube, centrifuged at 1200 rpm for 5–10 min at 4 °C, and the medium was removed. Organoids were broken up with a fire-polished pipette, centrifuged at 1200 rpm for 5–10 min at 4 °C, followed by mixing the pellet with Matrigel and plating in 50 µl droplets each 24-platewell. After solidification, 500 µl Complete Feeding Media (DMEM-F12 Advance, 100 × HEPES Buffer, 100 × Glutamax, 125 µg/mL Primocin, 20% R-Spondin conditioned medium, 500 nM A83-01, 50 ng/mL hEGF, 100 ng/mL mNoggin, 100 ng/mL hFGF10, 10 nM Gastrin I, 3 µM SB202190, 10 nM ProstaglandinE2, 1.25 mM N-acetylcysteine, 10 mM Nicotinammide, 1X B-27 Supplement) was added.

Organoids were cryopreserved in Recovery Cell Culture Freezing Medium (Thermo Fisher, America) as master and working biobanks.

Cell culture

Human colonic cell Caco-2 was acquired from the American Type Culture Collection (American, catalogue number: TCHu146). Caco-2 was cultured in DMEM High Glucose (Sigma, USA), supplemented with fetal bovine serum (10% v/v) (Sigma, USA), penicillin (50 U/ml) and streptomycin (50 U/ml). Incubation was in an environment of 37℃ and 5% CO2.

Real-time quantitative polymerase chain reaction (RT-qPCR)

TRIzol one step method (Applygen, China) was used to extract total RNA of Caco-2 cells, and Revert Aid First Strand cDNA Synthesis Kit (Thermo Fisher, America) was selected to reverse transcribe RNA into cDNA. We

used Power Up SYBR Green Master Mix (Lablead, China) to conduct RT-qPCR. The primer sequences were as follows: Human MCM2-F: 5'- ATGGCGGAATCATCGGAATCC -3', Human MCM2-R: 5'- GGTGAGGGCAT CAGTACGC -3', Human GAPDH-F: 5'- GGAGCGAGATCCCTCCAAAAT -3', Human GAPDH-R: 5'- GGCT GTTGTCATACTTCTCATGG -3'. GAPDH was used as the internal standard, RT-qPCR reaction was repeated for three times for each sample to ensure experimental repeatability.

Western blot analysis

A method described previously was used to extract total proteins of caco-2 cells and mouse colon tissue[8]. We collected the mucosa of the first 2 cm colon or Caco-2 cells and acquired the total protein as previously mentioned[23]. BCA assay (Lablead, China) was used to detect the protein concentration, and the extracts containing same amount of protein (15–30 μg) were transfered onto 4%-12% polyacrylamide gel for cataphoresis. Isolated protein was then transferred onto the PVDF membrane, which was non-specifically bound (5% bovine serum albumin in TBS-Tween 20 buffer), for 1 h at room temperature. 0.1% rabbit anti-CBS monoclonal antibody (CST, America), 0.1% rabbit anti-RPS20 monoclonal antibody (Proteintech, China), 0.1% rabbit anti-MCM2 monoclonal antibody (CST, America), 0.1% rabbit anti-GAPDH antibody (CST, America), and 0.1% rabbit anti-GAPDH monoclonal antibody (CST, America) were used to incubate the membrane for one night at 4℃. Afterwards, we used the secondary antibody to incubate the membrane for 1 h at room temperature, and finally used ECL detection reagent to perform the blots (Lablead, China).

Cell counting kit-8 assay

Cells were seeded into 96-well plates (5,000 cells/well). Cell viability was measured using Cell Counting Kit (CCK)-8 assay kits (Lablead, China) in accordance with the manufacturer's instructions. The optical density (OD at 450 nm) was measured using a microplate reader.

Biotin switch assay of sulfhydration

With reference to the method previously described, a modified biotin switch assay was used to detect the level of sulfhydration[24]. Briefly, HEN buffer (HEPES–NaOH pH 7.7 250 mM) with neocuproine (0.1 mM), EDTA (1 mM)) with protease/phosphatase inhibitors, 1% Nonidet-P40 (NP-40), and 150 l M deferoxamine were utilized to homogenize the cells or tissue samples. The homogenized samples were sonicated and centrifuged at 13,000 g at 4 ℃ for 20 min, then we added HEN buffer with 20 mM methyl thiosulfonate (MMTS) and 2.5% SDS to the lysate and shook for 30 min at 50 ℃. Acetone was added afterwards to remove MMTS. Meanwhile, we precipitated the protein for 1 h at 20 ℃. HEN buffer with 4 mM biotin-HPDP and 1% SDS was used to resuspend the pellets. After incubating at 25 ℃ for 3 h, acetone was used to purify the protein. In the end, we dissolved the protein in solution buffer and purified it with streptavidin-agarose beads, the sulfhydrated protein was examined by Western blot. Negative controls were from cells treated by dithiothreitol (DTT) (1 mmol/L).

CRISPR/Cas9 mediated knockout of CBS in cells

The CRISPR/Cas9 system was used to achieve stable knockout of the CBS gene in Caco-2 cells. In short, the interference target sgRNA was designed according to the sequence of the CBS gene as follows: CTGATGAG ATCCTGCAGCAG. We phosphorylated, annealed, and cloned the guide oligonucleotide into the BsmBI site of the pHBLV-U6-gRNA-EF1-CAS9-PURO vector (Hanheng Biotechnology, China), and then verified the constructed vector by sequencing. The transferred plasmid with the guide oligonucleotide was then transformed into E. coli DH5a, and was isolated from the bacteria using a plasmid DNA purification kit (Tiangen, China). The transferable lenti-CAS-puro plasmid, packaging plasmids psPAX2 and pMD2G (Hanheng Biotechnology, China) were transfected into 293T cells to produce lentivirus. 48 and 72 h after transfection, the virus-containing supernatant was collected and then used to transfect Caco-2 cells. After 24 h of infection, the medium in each plate was replaced with fresh medium containing puromycin (30 mg/L) for 24 h, and then with fresh medium for 24 h. Three times of repetition were done. Finally, puromycin-resistant Caco-2 cells were collected and western blot was used to detect the CBS knockout efficiency.

Transcriptome sequencing was performed after cells were collected, and the sequencing data has been uploaded to NCBI database (GEO: GSE276745 https://www.ncbi.nlm.nih.gov/geo/query/acc.cgi?acc=GSE276745).

Plasmid transfection

Plasmids pCDH-CMV-MCS-EF1-CopGFP-T2A-Puro-RPS20^{WT} (RPS20^{WT}), pCDH-CMV-MCS-EF1-CopGFP-T2A-Puro-RPS20^{C36A} (RPS20^{C36A}) and pCDH-CMV-MCS-EF1-CopGFP-T2A-Puro-RPS20^{C70A} (RPS20^{C70A}) were purchased from Mailgene Corporation (Beijing, China). DNA sequencing was used to confirm that Cys36 and Cys70 were successfully point-mutated to alanine. The relevant plasmids were transfected into Caco-2 WT cells using Lipofectamine 3000 (Lablead, China) according to Mailgene's recommendation. After 24 h of transfection, the medium containing plasmids was replaced with fresh medium for 2-3 days. Cells transfected with empty plasmid pCDH-CMV-MCS-EF1-CopGFP-T2A-Puro (Vector) were used as negative controls.

ActD chase assay

For ActD (MCE, USA) tracking assay, we treated Caco-2 WT, RPS20 C36A and RPS20 C70A cells with ActD alone (10 lg/ml) or with GYY4137 (50 μM) in serum-free medium. We collected cells every hour for 6 h and detected MCM2 mRNA expression using RT-qPCR. The MCM2 mRNA expression corresponding to different time points were calculated as the fold change relative to baseline.

Statistical analysis

One-way ANOVA and two-tailed Student's t-test (unpaired) were used to analyze the differences in mean values among groups (GraphPad Prism version 8.0 for Windows, GraphPad Software, America). P value < 0.05 was considered statistically significant, and all results were expressed as mean ± SD. All experiments were repeated for at least three times to ensure repeatability, and standard deviations were shown by error bars. * P < 0.05, ** P < 0.01, vs control group. # P < 0.05, ## P < 0.01, vs DSS group. △ P < 0.05, △△ P < 0.01, WT vs CBS +/− or CBS KO group.

Results

H_2S mitigated clinical symptoms and preserved survival rates in experimental colitis.

Verifying the knockdown of the CBS gene, western blot analysis showed a decrease in CBS expression in CBS +/− mice colon compared to WT (wild type) mice (Fig. 1A, B; SI, Fig. S2A). During the establishment of the UC model, mice were provided with 3.5% DSS in drinking water for 7 days, followed by regular water for 14 days (Fig. 1C). Compared with the Control group, the survival rate of DSS group mice was reduced, and the CBS +/− mice showed an even significant decrease of survival rate. GYY4137 improved the survival rate of both WT and CBS +/− mice after DSS induction (Fig. 1D, E). Meanwhile, the weight of WT mice was significantly decreased at day 6–21 and at day 4–21 in CBS +/− mice after DSS induction. Intraperitoneal injection of GYY4137 could significantly eased the weight loss from day 6–12 in WT mice and from day 6–17 in CBS +/− mice after DSS induction (Fig. 1F, G). Compared to WT mice, CBS +/− mice showed a more significant decreased of weight from day 12–17 in DSS group (Fig. 1H), but there was no significant weight difference between WT and CBS +/− mice in DSS + GYY4137 group (Fig. 1I). To further explore the effect of CBS-H_2S axis in UC, DAI score was used. In DSS group during day 1–21, compared to the control group, DAI was continuously increased through day 4–16 for WT mice and through day 4–18 for CBS +/− mice. The DAI score of DSS + GYY4137 group was lower than DSS group at day 4–14 in WT mice and at day 5–7, day 9 and day 13–15 in CBS +/− mice, which indicated that GYY4137 can lessen the increase of DAI score in mice after DSS induction (Fig. 1J, K). Together, these results indicated that H_2S alleviated the damage induced by DSS, and CBS gene knockdown aggravated intestinal injury in UC mice model.

H_2S improved the pathological changes of colon epithelium in colitis induced by DSS

To evaluate the histological injuries in intestinal epithelium, H&E staining of mouse colon Swiss roll and FD-4 flux assays were utilized to evaluate the damage on colon barrier. The H&E staining of colon epithelium in control group showed no inflammation and crypt damage, and after 7 days of DSS treatment, significant inflammation and crypt damage were observed in the colon. However, GYY4137 attenuated the damage to colon epithelium caused by DSS (Fig. 2A, B). Inflammation score was used to assess the damage of intestinal epithelium in each group (Fig. 2C–F). The results indicated that compared with control mice, DSS treatment aggravated the intestinal inflammation score in mice colon epithelium, and GYY4137 reduced the intestinal epithelium injury after DSS treatment (Fig. 2C, D). Compared to WT mice, the intestinal inflammation score was higher in CBS +/− mice in DSS group and DSS + GYY4137 group (Fig. 2E, F). CBS +/− mice, compared to WT mice, showed a higher FD-4 serum concentration after 7 days in DSS group. Meanwhile, compared to DSS group, the concentration of FD-4 in the DSS + GYY4137 group mice was significantly reduced. In both the DSS group and the DSS + GYY4137 group, CBS +/− mice displayed higher intestinal epithelial permeability compared with WT mice (Fig. 2G). These results suggested that H_2S mitigated the damage induced by DSS, and CBS-H_2S axis maintains intestinal barrier integrity and permeability disruption in UC mouse models.

H_2S sustained colonic epithelial repair function in DSS induced colitis

Ki67 immunohistochemical staining of colon tissue and colon length at day 7 were used as the proliferation index to evaluate colon repair. In control group, statistics showed that CBS knockdown did not significantly shorten the colon length of normally growing mice. Both WT and CBS + /- mice in the DSS group showed significant colon shortening, and the colon length of CBS + /- mice was significantly lower than WT group in DSS group. Administration of GYY4137 significantly reduced colon shortening, but there was no length difference between WT and CBS +/− mice in DSS + GYY4137 group (Fig. 2H, I). Lower colon tissue Ki67 IHC staining showed that Ki67 in the colonic epithelium was lower in CBS +/− mice than that in WT mice (Fig. 2J, K). These results revealed that CBS-H_2S axis maintained colon epithelial repair and proliferation after damages.

CBS-H_2S-axis maintained the growth and proliferation of colon organoids

To further investigate the effect of H_2S on the proliferation in mouse colon epithelium, colon organoids were cultured. Intestinal epithelial cells from WT and CBS +/− mice colon were selected to cultured colon organoids form day 0–10, and epithelial cells started to form organoids at day 2 (Fig. 3A, B). Colon organoids began to sprout on day 4 in WT group (Fig. 3A), and on day 6 in CBS +/− group (Fig. 3B). The number of organoids reached its maximum on day 8 and began to perish thereafter. At day 6 and 8, the total number of organoids in the WT group was significantly higher than that in CBS +/− group, but there was no significant difference statistically in the number of organoids at day 2, 4, 10 (Fig. 3C). Budding of organoids was regarded as an indicator of stemness, the number of total budding organoids reached its maximum at day 10, and the total number of budding organoids in the WT group was higher than that in the CBS +/− group at day 8. However, there was no statistical difference in the number of organoids at day 2, 4, 6, 10 (Fig. 3D). The number of single budding organoids in the WT group was significantly higher than that in the CBS +/− group on day 8, but there was no statistically difference in the number of single organoids at day 2, 4, 6, 10 (Fig. 3E). The number of multiple budding organoids was also higher in the WT group at day 8 and 10 (Fig. 3F), as well as its percentage (Fig. 3G, H). Cyst-like organoid is the indicator of defect, while a higher proportion and quantity of defective

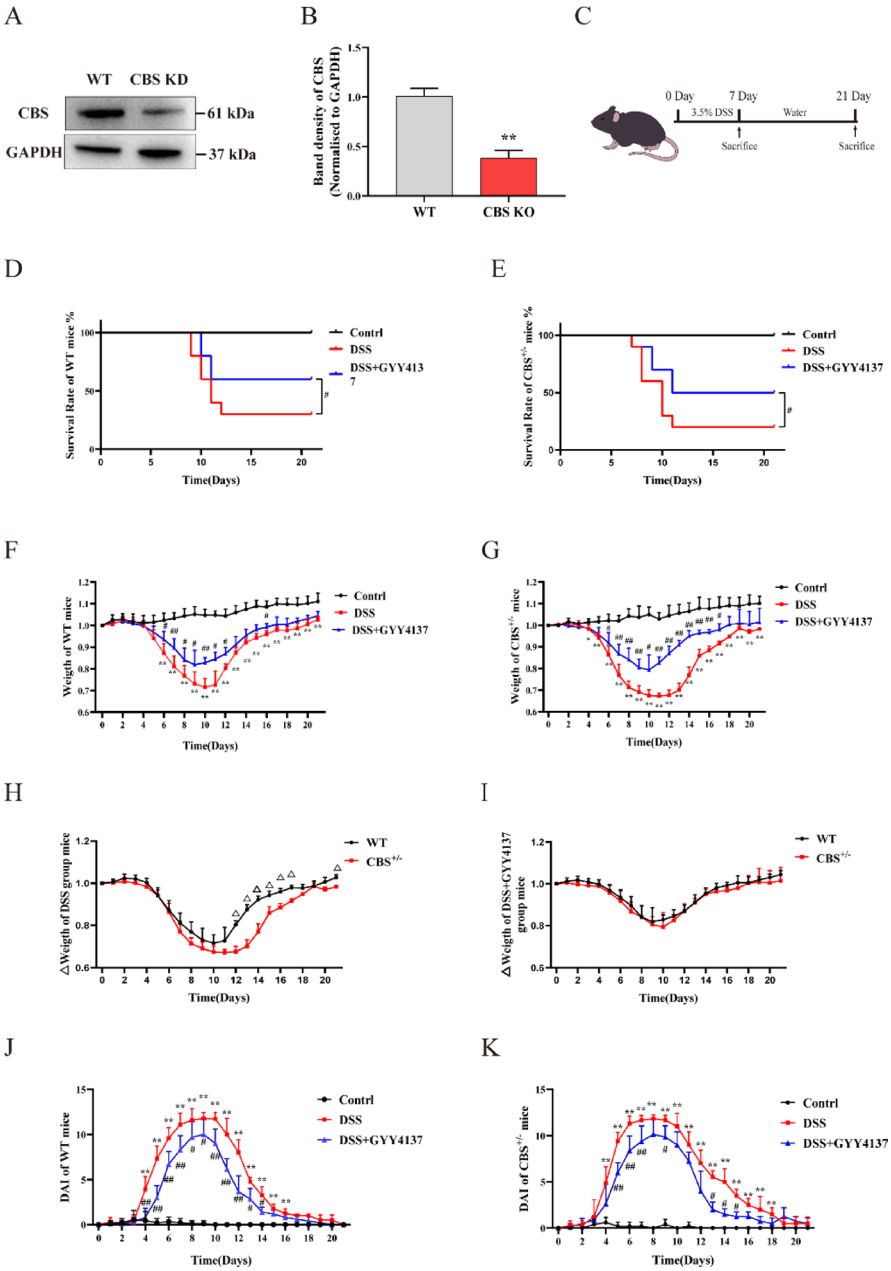

Fig. 1. CBS knockdown exaggerated experimental colitis induced by DSS. (**A**) Representative western blot images of CBS in mice colon epithelial cells. (**B**) Relative band density of CBS in western blot. (**C**) Treatment overview of C57/BL mice induced by 3.5% DSS. (**D**, **E**) Survival rate of WT and CBS +/− mice. (**F**, **G**) Body weight changes of WT and CBS +/− mice. (**H**) Comparison of weights between WT and CBS + /- mice of DSS group. (**I**) Comparison of weights between WT and CBS +/− mice of DSS + GYY4137 group. (**J**, **K**) The DAI score of WT and CBS +/− mice.

organoids indicate poor growth status. The number of normal organoids in the WT group was significantly higher than that in the CBS group at day 6, 8, 10(Fig. 3G–K), and there was no statistical difference in the number of normal organoid at day 2, 4 (Fig. 3G, H, K). The number of defective organoids in the WT group was significantly higher than that in the CBS +/− group at day 10, and there were no statistical differences in the number of defective organoids at day 2, 4, 6, 8 (Fig. 3G, H, L). The result of FD-4 fluxes of WT and CBS +/− organoids at day 10 indicated H_2S maintained permeability of organoids (Fig. 3M). These results illustrated that CBS-H_2S axis maintained the growth and permeability integrity of colon epithelial organoid in mice.

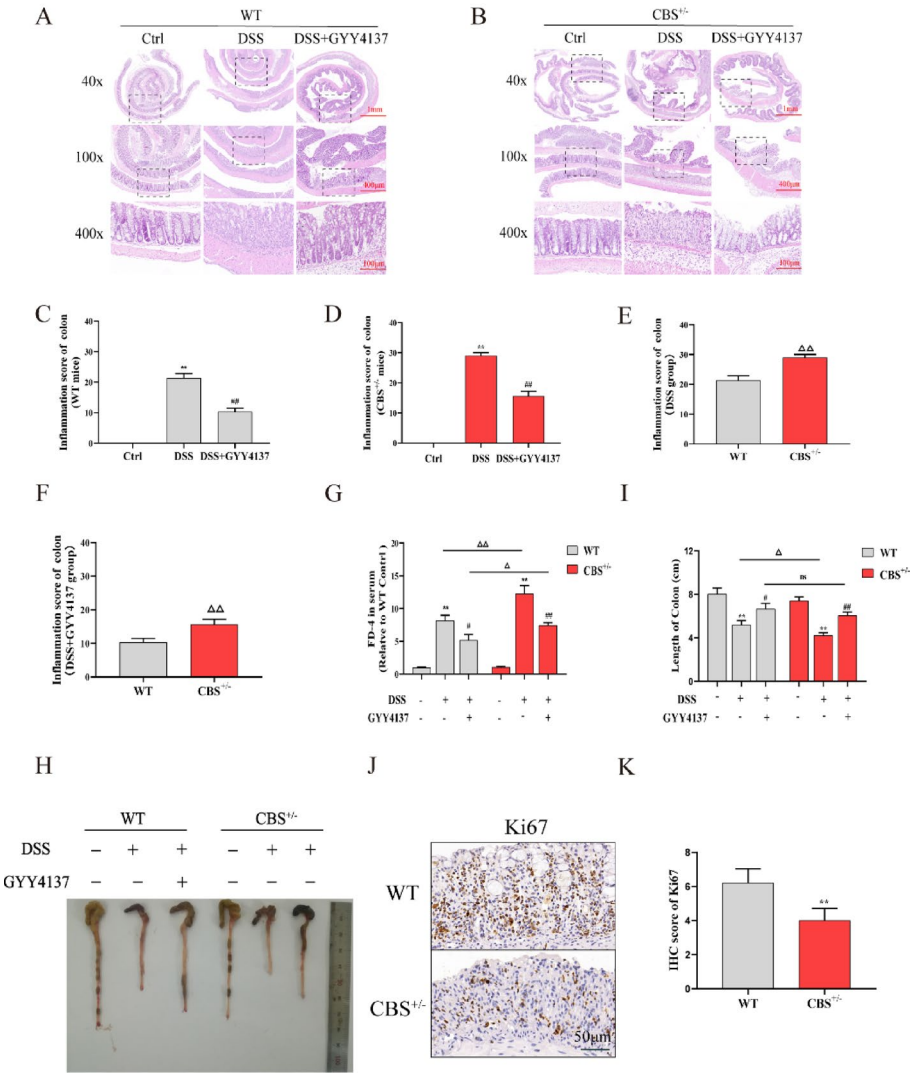

Fig. 2. CBS-H_2S axis alleviated intestinal barrier disruption and maintained intestinal epithelial proliferation in UC. (**A**, **B**) H&E staining of colon tissue of WT and CBS +/− mice at day 7 (40x, 100 × and 400x). (**C**, **D**) Inflammation score of colon tissue of WT and CBS + /- mice. (**E**, **F**) Comparison of inflammation score of colons between WT and CBS +/− mice in DSS group and DSS + GYY4137 group. (**G**) FD-4 flux of intestine of WT and CBS +/− mice at day 7. (**H**, **I**) Colon length between WT and CBS +/− mice at day 7. (**J**, **K**) Ki67 IHC staining of lower colon (near rectum) epithelial tissue between WT and CBS +/− mice induced by DSS after 7 days.

H_2S maintained MCM2 expression by sulfhydrating RBPs

To investigate the effect of H_2S on cells proliferation related pathways, Caco-2 CBS KO cells and Caco-2 WT cell were used for transcriptome sequencing. To verify the knockout of the CBS gene, western blot was performed with images showing a decrease in CBS expression in Caco-2 CBS KO cells compared with Caco-2 WT cells (Fig. 4A, B; SI, Fig. S2B). The KEGG enrichment pathway of transcriptome sequencing results exhibited significant differences in DNA replication pathways (Fig. 4C). GSEA indicated that CBS KO decreased the expression of MCM2 (Fig. 4D). MCM2 expression was significantly lower in the colon of CBS +/− mice than WT mice after treatment of DSS (SI, Fig. S1B). Western blot also showed a decrease in MCM2 expression in Caco-2 CBS KO cells (Fig. 4E, F SI, Fig. S2C). Studies have proven that MCM2 is closely related to the proliferation and growth of tumor cells and normal cells[14,15,17], and the stability of mRNA is closely related to RNA-binding proteins. Based on the findings above, we hypothesized that H_2S affects the expression of MCM2 mRNA by changing the sulfhydration level of RNA-binding protein of MCM2 mRNA. To confirm this hypothesis, mass spectrometry was employed to determine differences in protein sulfhydration levels in Caco-2 WT cells and Caco-2 CBS KO cells with or without GYY4137(Fig. 4G). At the same time, the catRAPID database was used as reference to predict the RNA-binding protein (RBPs) of MCM2 mRNA (http://s.tartaglialab.com/page/catrapid_group). Compared with Caco-2 WT cells, MCM2 RBPs' sulfhydration levels of RPS20 was found to be reduced by over

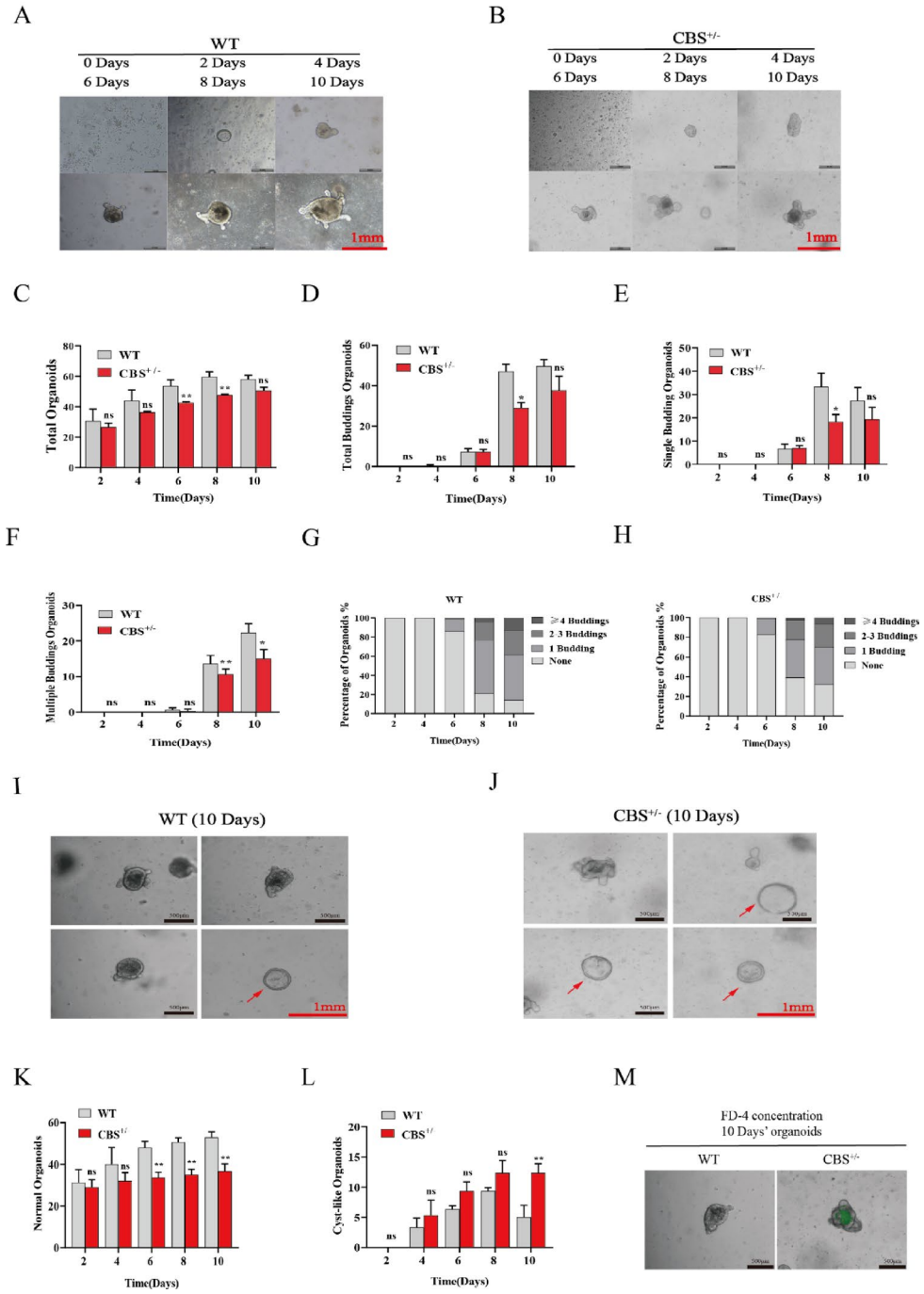

Fig. 3. CBS-H_2S axis sustained proliferation of intestinal epithelial organoids in mice. (**A**, **B**) Colon intestinal tissue organoids growth status of WT and CBS +/− mice. (**C**) The number of total organoids statistics of WT and CBS +/− mice from day 2–10. (**D**) The number of total buddings organoids of WT and CBS +/− mice from day 2–10. (E) The number of single budding organoids of WT and CBS +/− mice from day 2–10. (**F**) The number of multiple budding organoids of WT and CBS +/− mice from day 2–10. (**G**, **H**) The percentage of organoids of WT and CBS +/− mice from day 2–10. (**I**, **J**) The Cyst-like organoids of WT and CBS +/− mice at day 10. (**K**, **L**) The statistics of normal and cyst-like organoids of WT and CBS +/− mice from day 2–10. (**M**) FD-4 flux of WT and CBS +/− organoids at day 10.

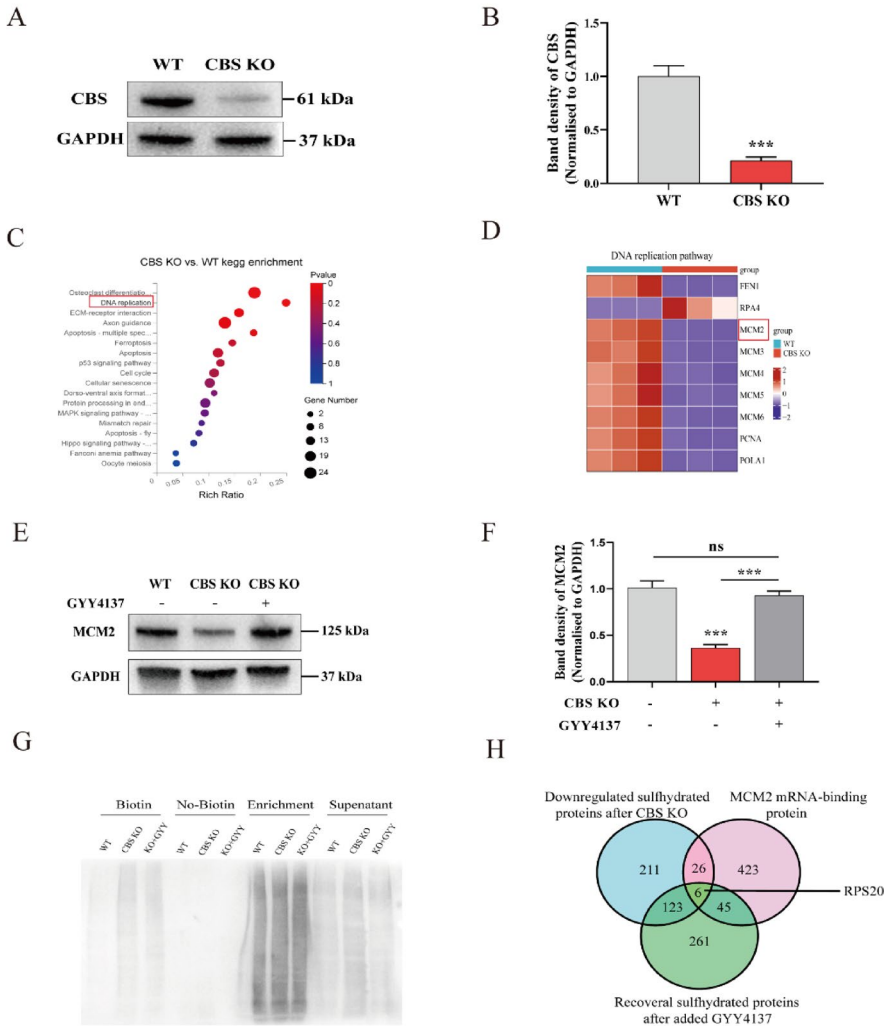

Fig. 4. CBS-H_2S-axis maintained expression of MCM2 in colon epithelium. (**A**, **B**) Western blot images and band density of CBS in Caco-2 WT cells and Caco-2 CBS KO cells. (**C**) Differentially expressed genes pathway in Caco-2 WT cells and Caco-2 CBS KO cells. (**D**) Differentially expressed genes of DNA replication pathway in Caco-2 WT cells and Caco-2 CBS KO cells. (**E**, **F**) Western blot images and band density of MCM2 in Caco-2 WT cells and Caco-2 CBS KO cells with or without GYY4137. (**G**) Caco-2 WT cells and Caco-2 CBS KO cells with or without GYY4137for 48 h before modified biotin switch assays. Bands in the respective lanes in SDS-PAGE gels were collected for mass spectrometry. (**H**) Take the intersection of proteins with more than 50% change in sulfhydration level and MCM2 RNA-binding protein.

50% after CBS KO, and restored to over 100% after the addition of GYY4137 (Fig. 4H). These results indicated that sulfhydration level of MCM2 RBP mediated by H_2S may affects the expression level of MCM2.

H_2S improved the expression of MCM2 by sulfhydration of RPS20

Western blotting showed no difference of RPS20 expression in mice colon among Control, DSS and DSS + GYY4137 group, but level of sulfhydrated RPS20 significantly depressed in DSS group and the level of RPS20-ssh significantly recovered after intraperitoneal injection of GYY4137. However, MCM2 expression in sulfhydrated RPS20 protein showed no significant difference between WT and CBS +/− mice (Fig. 5A–E; SI, Fig. S3A, B). To verify the effect of CBS KO on cell growth, CCK-8 was utilized to evaluate cell viability, and the results showed that at 24, 48, 72 h, the proliferation level of Caco-2 CBS KO cells was significantly lower than that of the Caco-2 WT cells. When Caco-2 CBS KO cells were cultured in medium containing GYY4137, the proliferation status significantly improved at 48 and 72 h (Fig. 5F). The result of Western blot showed a greater decrease in RPS20-ssh expression in Caco-2 CBS KO cells compared with Caco-2 WT cells, and the expression of RPS20-ssh level was recovered with the addition of GYY4137 (Fig. 5G, H) SI, Fig. S2D).

Protein sequence of RPS20 was obtained from NCBI, and shown that RPS20 has two cysteine sites, Cys36 and Cys70. In order to further investigate the maintenance effect of sulfhydrated RPS20 on the expression of

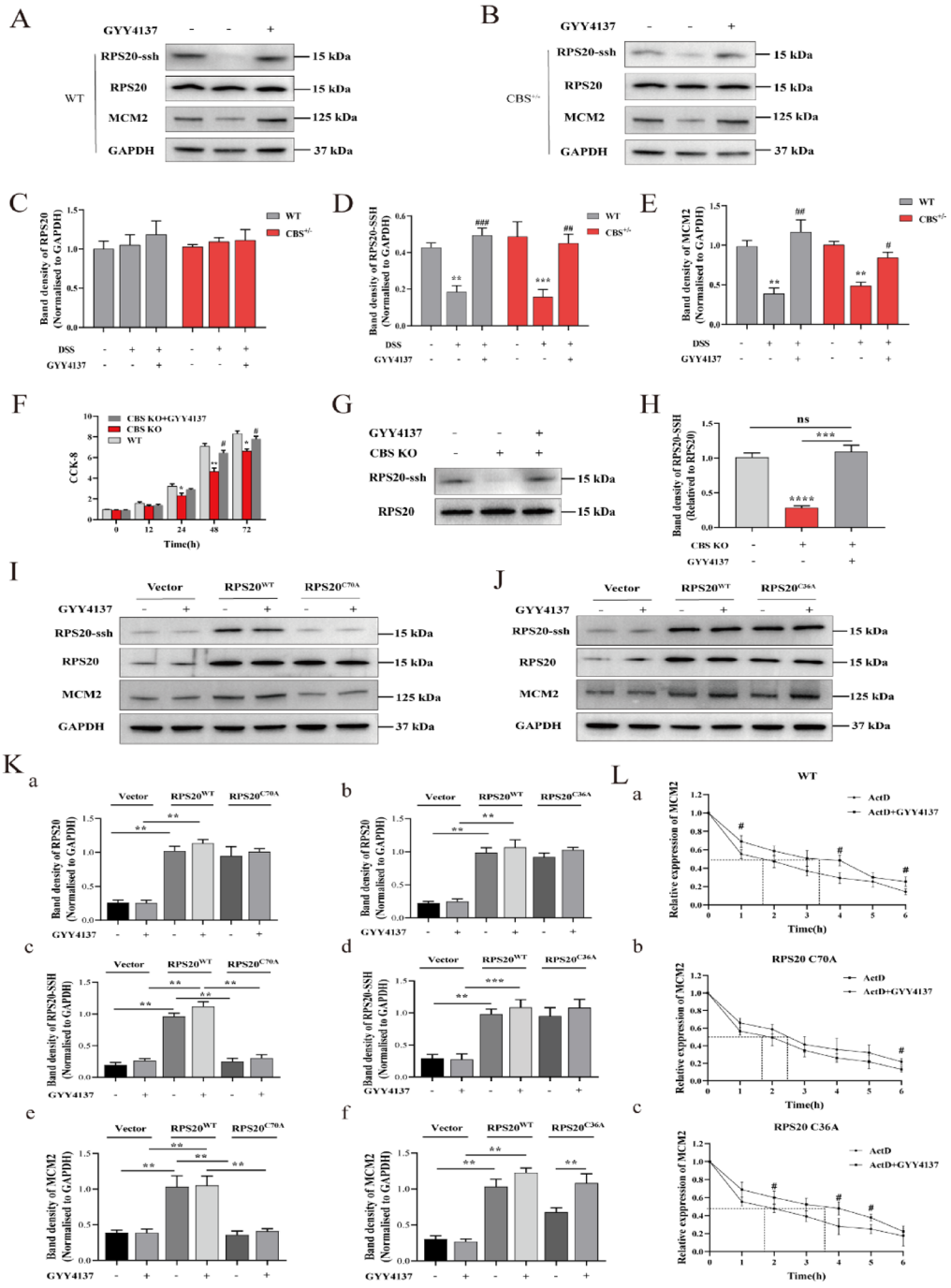

Fig. 5. CBS-H_2S axis sustained the stability of MCM2 mRNA as well as the expression level of MCM2 by sulfhydrating RPS20. (**A**, **B**) Representative western blot images of MCM2, RPS20 and RPS20-ssh in colon epithelium cells of WT and CBS +/− mice. (**C**, **D**, **E**) Relative band intensity of MCM2, RPS20 and RPS20-ssh in mice. (**F**) Cell viability of Caco-2 WT cells and Caco-2 CBS KO cells with or without GYY4137. (**G**, **H**) Western blot of RPS20-ssh in Caco-2 WT cells and Caco-2 CBS KO cells with or without GYY4137 for 48 h. (**I**, **J**) Western blot analysis of RPS20, RPS20-ssh and MCM2 in Caco-2 cells after transfected plasmid. (**K**) Relative band intensity of RPS20, RPS20-ssh and MCM2. (**L**) ActD chase assays for the stability of MCM2 mRNA in Caco-2 cells treated with or without GYY4137. (**a**) Stability of MCM2 mRNA in WT Caco-2 cells. (**b**) Stability of MCM2 mRNA in $RPS20^{C70A}$ Caco-2 cells. (**c**) Stability of MCM2 mRNA in $RPS20^{C36A}$ Caco-2 cells. * P < 0.05, ** P < 0.01, *** < 0.001, **** < 0.0001, vs WT group. # P < 0.05, ## P < 0.01, vs CBS KO or ActD group.

MCM2, and to clarify the cysteine site of H_2S in RPS20, empty plasmid (Vector), plasmids expressing RPS20 ($RPS20^{WT}$), plasmid with RPS20 Cys36 single-point mutation to alanine ($RPS20^{C36A}$) and plasmid with RPS20 Cys70 single-point mutation to alanine ($RPS20^{C70A}$) were transfected into Caco-2 WT cells. Western blotting images of Caco-2 cells demonstrated that the overexpression of $RPS20^{WT}$, $RPS20^{C36A}$ and $RPS20^{C70A}$ increased the expression of RPS20. However, overexpression of $RPS20^{C70A}$ did not increase the expression of RPS20-ssh, and GYY4137 failed to improve the expression of MCM2 transfected with $RPS20^{C70A}$. GYY4137 also failed to sulfhydrate RPS20 expressed in Caco-2 cells overexpression with $RPS20^{C70A}$ (Fig. 5I–K; SI, Fig. S3C, D). These results revealed that H_2S maintains MCM2 expression by sulfhydrating the RPS20 Cyst70 site to support cell proliferation. ActD tracking assay was performed to further explore MCM2 mRNA stability in Caco-2 cells. The assay showed that after treated with ActD alone in WT cells, the half-life of MCM2 mRNA was approximately 1.6 h, and with the addition of GYY4137, the half-life became approximately 3.4 h. In the $RPS20^{C36A}$ group, the half-life was approximately 1.7 h, and became approximately 3.6 h after GYY4137 added. In the $RPS20^{C70A}$ cells, the half-life was approximately 1.8 h, and 2.5 h after GYY4137 added (Fig. 5L). ActD tracking assay further showed that H_2S acts on the RPS20 Cys70 site to maintain the stability of MCM2 mRNA. These results suggested that H_2S-mediated sulfhydration of RPS20 might be the mechanism of how CBS-H_2S axis maintains intestinal epithelial cell proliferation in DSS-induced colitis.

Discussions

As the primary guardian of homeostasis, the intestinal barrier has evolved into a multilayered system, serving as both a physical and a functional barrier against the invasion of harmful substances into the body. Increased intestinal epithelial permeability caused by intestinal barrier damage is associated with the occurrence and development of various diseases, such as colitis, bacterial translocation, systemic inflammatory response syndrome[25]. During colitis, a large amount of toxic substances or bacteria in the intestine enter the internal environment, which further aggravates the destruction of the intestinal barrier and delays the repair of intestinal epithelium[26]. Identifying protective agents for intestinal barrier proliferation and promoting intestinal epithelial repair may provide potential therapeutic strategies for colitis.

H_2S plays a pivotal role in the pathogenesis of numerous diseases, spanning inflammatory conditions to cancers[27,28]. The supportive effect of exogenous H_2S on cell proliferation ability has been verified[29,30]. The protective effect of exogenous H_2S on the intestinal barrier has been reported, but excessively high concentration of H_2S has brought adverse effects, such as inhibiting intestinal epithelial cell proliferation through cell cycle arrest[12,31–34]. Our previous study found that CBS expression was decreased in UC lesion sites, indicating that CBS knockdown amplified TNF-α/IFN-γ-induced barrier damage in Caco-2 monolayers, and H_2S inhibits COX-2 expression by sulfhydrating HuR, protecting the integrity of intestinal barrier function and inhibiting intestinal inflammation[10,35]. However, the effect of CBS-H_2S axis on intestinal barrier repair in UC and its underlying mechanism remain to be explored.

In this study, experimental colitis was induced by 3.5% DSS in WT and CBS +/− mice. The results indicated that after the treatment of DSS, the body weight of CBS +/− mice decreased faster compared with WT mice and the recovered slower. WT mice had significantly lower increases in DAI scores than CBS +/− mice, and the DAI score during the recovery period was significantly faster than that of CBS +/− mice. Histological evaluation of the colon demonstrated increased disruption of intestinal epithelial tissue in CBS knockdown mice. A more significant increase in intestinal permeability was also noted, together with a significantly higher degree of fibrosis in the colon epithelium. Intraperitoneal injection of GYY4137 could significantly reduce the degree of fibrosis. At the same time, the colon length of CBS knockdown mice was shorter than that of WT mice after DSS treatment, and GYY4137 alleviated colon shortening. Compared with WT mice, the proliferation ability of colonic epithelium in CBS +/− mouse colitis model was significantly reduced. Interestingly, compared with WT mice, CBS +/− mice colon showed more severe intestinal fibrosis after treated with DSS, and administration of GYY4137 alleviated fibrosis (Fig. S1D, E).

Organoid technology can effectively expand intestinal epithelial tissue in vitro, and organoids can be used to replace native colon epithelium to produce functional intestinal crypt[36]. In our study, mouse colon epithelial cells were used to culture organoids. The results indicated that the overall number of organoids, single budding organoids and multiple budding organoids in the WT group during the growth process were significantly higher than those of the organoids in the CBS +/− group. The study also figured that in the CBS +/− group, the percentage of Cyst-like Organoids was significantly higher than that in the WT group. Meanwhile, the permeability to FD-4 of organoids in the CBS +/− group was significantly higher than that of the WT group. Animal experiments and organoid results indicated that the CBS-H_2S axis protects intestinal barrier and maintains intestinal epithelial growth and proliferation. Given the above results, we set out to study the mechanism by which H_2S maintains intestinal epithelial proliferation in UC.

RNA-binding proteins (RBPs) are key trans factors associated with specific cis elements present in mRNAs and regulate their stability and translation[37,38]. Previous studies conducted by our research group have demonstrated that H_2S can increase sulfhydrated HuR, leading to the degradation of COX-2 mRNA and, consequently, a reduction in inflammation[10]. Ribosomal protein S20 (RPS20) is a member of the S10P family of ribosomal proteins, and its main function lies in the regulation of ribosomal RNA processing[39]. Unlike other RPs, which are usually found in the nucleus[40–42], RPS20 is primarily located in the cytoplasm[43]. RPS20 is involved in the occurrence and development of various tumors[39,44]. Recent studies have shown that RPS20 is also involved in non-ribosomal regulation, and also in the regulation of p53-mouse double minute 2 homologous signaling pathway[45,46]. In addition, RPS20 has been shown to interact with GNL1 to regulate cell proliferation[47]. CatRAPID database predicts that RPS20 is one of the RNA-binding proteins of the MCM2 mRNA (s.tartaglialab.com/page/catrapid_group). However, it is still unknown whether RPS20 is involved in the regulation of MCM2 gene

expression and thereby regulates the repair and proliferation of intestinal epithelium in experimental ulcerative colitis.

Based on previous reports and the results above, we hypothesized that H_2S could increase the stability of RPS20 through sulfhydration of RPS20, thereby promoting the expression of MCM2. Our experiments showed that in DSS-induced ulcerative colitis colonic epithelium, MCM2 expression was reduced in the intestinal epithelial tissue of WT and CBS +/− mice, with no change in total RPS20 level expression. After injected GYY4137, the expression of MCM2 increased significantly, but the total expression of RPS20 did not change significantly. We detected the sulfhydration level of RPS20 through biotin switch assay and western blotting, and results indicated that compared with Control mice, the level of sulfhydration of RPS20 in mice in the DSS group was significantly reduced. When injected GYY4137 on the basis of DSS treatment, the sulfhydration of RPS20 increased significantly. CRISPR/Cas9 was used to knock out the CBS gene in Caco-2 cells. Western blotting results showed that CBS knockout reduced sulfhydrated RPS20 and MCM2, and the total expression of RPS20 remained unchanged. We further investigated the specific sites where H_2S interacts with RPS20, and western blot results indicated H_2S sulfhydrated RPS20 Cys70 rather than RPS20 Cys36, thereby increasing RPS20-ssh levels, MCM2 mRNA stability and MCM2 expression. In addition, we tested the stability of MCM2 mRNA in Caco-2 cells through ActD tracking assay and found that H_2S significantly increased the stability of MCM2 mRNA in Caco-2 cells. The results of the mRNA stability experiment also indicated that H_2S increases the stability of MCM2 mRNA by sulfhydrating RPS20 Cys70. Results above indicated CBS-H_2S axis maintained the expression of MCM2 and the stability of MCM2 mRNA by increasing the sulfhydration of RPS20, which may be one of the potential mechanisms by which H_2S sustained epithelial proliferation in UC. H_2S increased the affinity of RPS20 and MCM2 mRNA by increased RPS20-ssh, then increased the binding of RPS20 and MCM2 mRNA, thereby prevented MCM2 mRNA degradation, promoted MCM2 expression and ultimately maintained intestinal epithelial proliferation.

In our study, we applied some novel methods in vitro and in vivo. We established a CBS knockdown mouse strain and verified the protective effect of the CBS-H_2S axis on intestinal epithelial proliferation in mice in DSS-induced colitis. We selected mouse colon epithelial cells for organoid culture and confirmed that CBS-H_2S maintained the growth and proliferation of mouse colon organoids. We further determined the specific cysteine site where H_2S acts in RPS20 in human cell lines. Nevertheless, while this study substantiated the involvement of the CBS-H_2S axis in mouse intestinal epithelium and human cell lines, a limitation lies in the absence of experiments conducted on human colitis tissue.

In summary, our study demonstrated that the CBS-H_2S axis plays a crucial role in protecting intestinal barrier repair function in DSS-induced UC and demonstrated the promotion of MCM2 mRNA stability by increasing sulfhydrated RPS20. This may be one of the mechanisms by which the CBS-H_2S axis maintained intestinal epithelial proliferation on UC and other colitis. And we provide a potential therapy for the treatment of colitis.

Ethics

This study followed all institutional and national guidelines for the care and use of animals. All mouse experiments were approved by the Animal Ethics Committee of Peking University First Hospital (No. J2022082).

Data availability

The authors confirm that the data supporting the findings of this study are available within the article and its supplementary materials. And the RNA-seq data supporting the findings of this study have been uploaded to a public database (https://www.ncbi.nlm.nih.gov/geo/query/acc.cgi?acc=GSE276745).

Received: 3 October 2024; Accepted: 12 May 2025
Published online: 21 May 2025

References

1. Minton, K. Intestinal barrier protection. *Nat. Rev. Immunol.* **22**, 144–145. https://doi.org/10.1038/s41577-022-00685-5 (2022).
2. Dong, L. et al. Mannose ameliorates experimental colitis by protecting intestinal barrier integrity. *Nat. Commun.* **13**, 4804. https://doi.org/10.1038/s41467-022-32505-8 (2022).
3. France, M. M. & Turner, J. R. The mucosal barrier at a glance. *J. Cell Sci.* **130**, 307–314. https://doi.org/10.1242/jcs.193482 (2017).
4. Brandt, A. et al. Impairments of intestinal arginine and NO metabolisms trigger aging-associated intestinal barrier dysfunction and 'inflammaging'. *Redox Biol.* **58**, 102528. https://doi.org/10.1016/j.redox.2022.102528 (2022).
5. Szabo, C. Gasotransmitters in cancer: From pathophysiology to experimental therapy. *Nat. Rev. Drug Discov.* **15**, 185–203. https://doi.org/10.1038/nrd.2015.1 (2016).
6. Schlapbach, L. J. et al. Effect of nitric oxide via cardiopulmonary bypass on ventilator-free days in young children undergoing congenital heart disease surgery: The NITRIC randomized clinical trial. *JAMA* **328**, 38–47. https://doi.org/10.1001/jama.2022.9376 (2022).
7. Cirino, G., Szabo, C. & Papapetropoulos, A. Physiological roles of hydrogen sulfide in mammalian cells, tissues, and organs. *Physiol. Rev.* **103**, 31–276. https://doi.org/10.1152/physrev.00028.2021 (2023).
8. Chen, S. et al. Decreased expression of cystathionine β-synthase exacerbates intestinal barrier injury in ulcerative colitis. *J. Crohns Colitis* **13**, 1067–1080. https://doi.org/10.1093/ecco-jcc/jjz027 (2019).
9. Te Winkel, J. et al. Mesenchymal stem cells promote mesenteric vasodilation through hydrogen sulfide and endothelial nitric oxide. *Am. J. Physiol. Gastrointest. Liver Physiol.* **317**, G441–G446. https://doi.org/10.1152/ajpgi.00132.2019 (2019).
10. Guo, S. et al. CBS-H_2S axis preserves the intestinal barrier function by inhibiting COX-2 through sulfhydrating human antigen R in colitis. *J. Adv. Res.* **44**, 201–212. https://doi.org/10.1016/j.jare.2022.03.010 (2023).
11. Bibli, S. I. et al. Cystathionine γ lyase sulfhydrates the RNA binding protein human antigen R to preserve endothelial cell function and delay atherogenesis. *Circulation* **139**, 101–114. https://doi.org/10.1161/circulationaha.118.034757 (2019).
12. Streeter, E., Ng, H. H. & Hart, J. L. Hydrogen sulfide as a vasculoprotective factor. *Med. Gas Res.* **3**, 9. https://doi.org/10.1186/2045-9912-3-9 (2013).

13. Ma, J. et al. GYY4137-induced p65 sulfhydration protects synovial macrophages against pyroptosis by improving mitochondrial function in osteoarthritis development. *J. Adv. Res.* https://doi.org/10.1016/j.jare.2024.05.033 (2024).
14. Xu, X., Hua, X., Brown, K., Ren, X. & Zhang, Z. Mcm2 promotes stem cell differentiation via its ability to bind H3–H4. *Elife* **11**, e80917. https://doi.org/10.7554/eLife.80917 (2022).
15. Zhou, X. et al. MCM2 promotes the stemness and sorafenib resistance of hepatocellular carcinoma cells via hippo signaling. *Cell Death Discov.* **8**, 418. https://doi.org/10.1038/s41420-022-01201-3 (2022).
16. Liao, X. et al. Distinct diagnostic and prognostic values of minichromosome maintenance gene expression in patients with hepatocellular carcinoma. *J. Cancer* **9**, 2357–2373. https://doi.org/10.7150/jca.25221 (2018).
17. Li, S. et al. ESRG is critical to maintain the cell survival and self-renewal/pluripotency of hPSCs by collaborating with MCM2 to suppress p53 pathway. *Int. J. Biol. Sci.* **19**, 916–935. https://doi.org/10.7150/ijbs.79095 (2023).
18. Yadav, P., Mishra, J. S., Hurt, M. W., Chen, D. B. & Kumar, S. H2S donor GYY4137 mitigates sFlt-1-induced hypertension and vascular dysfunction in pregnant rats. *Biol. Reprod.* **111**, 879–889. https://doi.org/10.1093/biolre/ioae103 (2024).
19. Cooper, H. S., Murthy, S. N., Shah, R. S. & Sedergran, D. J. Clinicopathologic study of dextran sulfate sodium experimental murine colitis. *Lab. Investig. J. Tech. Methods Pathol.* **69**, 238–249 (1993).
20. Raju, P. et al. Inactivation of paracellular cation-selective claudin-2 channels attenuates immune-mediated experimental colitis in mice. *J. Clin. Investig.* **130**, 5197–5208. https://doi.org/10.1172/jci138697 (2020).
21. Zhang, Y. et al. BAFF blockade attenuates DSS-induced chronic colitis via inhibiting NLRP3 inflammasome and NF-κB activation. *Front. Immunol.* **13**, 783254. https://doi.org/10.3389/fimmu.2022.783254 (2022).
22. Trilleaud, C. et al. Agonist anti-ChemR23 mAb reduces tissue neutrophil accumulation and triggers chronic inflammation resolution. *Sci. Adv.* **7**, eabd1453. https://doi.org/10.1126/sciadv.abd1453 (2021).
23. Moriez, R. et al. Myosin light chain kinase is involved in lipopolysaccharide-induced disruption of colonic epithelial barrier and bacterial translocation in rats. *Am. J. Pathol.* **167**, 1071–1079. https://doi.org/10.1016/s0002-9440(10)61196-0 (2005).
24. Lin, Z. et al. Hydrogen sulfide attenuates oxidative stress-induced NLRP3 inflammasome activation via S-sulfhydrating c-Jun at Cys269 in macrophages. *Biochim. Biophys. Acta Mol. Basis Dis.* **1864**, 2890–2900. https://doi.org/10.1016/j.bbadis.2018.05.023 (2018).
25. Wu, H., Huang, R., Fan, J., Luo, N. & Yang, X. Low potassium disrupt intestinal barrier and result in bacterial translocation. *J. Transl. Med.* **20**, 309. https://doi.org/10.1186/s12967-022-03499-0 (2022).
26. Rescigno, M. The intestinal epithelial barrier in the control of homeostasis and immunity. *Trends Immunol.* **32**, 256–264. https://doi.org/10.1016/j.it.2011.04.003 (2011).
27. Lo Faro, M. L., Fox, B., Whatmore, J. L., Winyard, P. G. & Whiteman, M. Hydrogen sulfide and nitric oxide interactions in inflammation. *Nitric Oxide* **41**, 38–47. https://doi.org/10.1016/j.niox.2014.05.014 (2014).
28. Youness, R. A. et al. Targeting hydrogen sulphide signaling in breast cancer. *J. Adv. Res.* **27**, 177–190. https://doi.org/10.1016/j.jare.2020.07.006 (2021).
29. Liu, Y. et al. Hydrogen sulfide maintains mesenchymal stem cell function and bone homeostasis via regulation of Ca^{2+} channel sulfhydration. *Cell Stem Cell* **15**, 66–78. https://doi.org/10.1016/j.stem.2014.03.005 (2014).
30. Shuang, T. et al. Interaction among estrogen, IGF-1, and H2S on smooth muscle cell proliferation. *J. Endocrinol.* **248**, 17–30. https://doi.org/10.1530/joe-20-0190 (2021).
31. Collin, M. et al. Inhibition of endogenous hydrogen sulfide formation reduces the organ injury caused by endotoxemia. *Br. J. Pharmacol.* **146**, 498–505. https://doi.org/10.1038/sj.bjp.0706367 (2005).
32. Xu, W., Watanabe, K., Mizukami, Y., Yamamoto, Y. & Suzuki, T. Hydrogen sulfide suppresses the proliferation of intestinal epithelial cells through cell cycle arrest. *Arch. Biochem. Biophys.* **712**, 109044. https://doi.org/10.1016/j.abb.2021.109044 (2021).
33. Beaumont, M. et al. Detrimental effects for colonocytes of an increased exposure to luminal hydrogen sulfide: The adaptive response. *Free Radic. Biol. Med.* **93**, 155–164. https://doi.org/10.1016/j.freeradbiomed.2016.01.028 (2016).
34. Blachier, F. et al. Changes in the luminal environment of the colonic epithelial cells and physiopathological consequences. *Am. J. Pathol.* **187**, 476–486. https://doi.org/10.1016/j.ajpath.2016.11.015 (2017).
35. Chen, S. W. et al. Protective effect of hydrogen sulfide on TNF-α and IFN-γ-induced injury of intestinal epithelial barrier function in Caco-2 monolayers. *Inflamm. Res.* **64**, 789–797. https://doi.org/10.1007/s00011-015-0862-5 (2015).
36. Sugimoto, S. et al. An organoid-based organ-repurposing approach to treat short bowel syndrome. *Nature* **592**, 99–104. https://doi.org/10.1038/s41586-021-03247-2 (2021).
37. Wu, X. & Xu, L. The RNA-binding protein HuR in human cancer: A friend or foe?. *Adv. Drug Deliv. Rev.* **184**, 114179. https://doi.org/10.1016/j.addr.2022.114179 (2022).
38. Gerstberger, S., Hafner, M. & Tuschl, T. A census of human RNA-binding proteins. *Nat. Rev. Genet.* **15**, 829–845. https://doi.org/10.1038/nrg3813 (2014).
39. Shen, C. et al. Biochemical and clinical effects of RPS20 expression in renal clear cell carcinoma. *Oncol. Rep.* **49**, 22. https://doi.org/10.3892/or.2022.8459 (2023).
40. Ko, J. R., Wu, J. Y., Kirby, R., Li, I. F. & Lin, A. Mapping the essential structures of human ribosomal protein L7 for nuclear entry, ribosome assembly and function. *FEBS Lett.* **580**, 3804–3810. https://doi.org/10.1016/j.febslet.2006.05.073 (2006).
41. Chen, I. J., Wang, I. A., Tai, L. R. & Lin, A. The role of expansion segment of human ribosomal protein L35 in nuclear entry, translation activity, and endoplasmic reticulum docking. *Biochem. Cell Biol.* **86**, 271–277. https://doi.org/10.1139/o08-032 (2008).
42. Antoine, M. et al. Identification of an unconventional nuclear localization signal in human ribosomal protein S2. *Biochem. Biophys. Res. Commun.* **335**, 146–153. https://doi.org/10.1016/j.bbrc.2005.07.069 (2005).
43. Tai, L. R., Chou, C. W., Wu, J. Y., Kirby, R. & Lin, A. Late-assembly of human ribosomal protein S20 in the cytoplasm is essential for the functioning of the small subunit ribosome. *Exp. Cell Res.* **319**, 2947–2953. https://doi.org/10.1016/j.yexcr.2013.09.013 (2013).
44. Nieminen, T. T. et al. Germline mutation of RPS20, encoding a ribosomal protein, causes predisposition to hereditary nonpolyposis colorectal carcinoma without DNA mismatch repair deficiency. *Gastroenterology* **147**, 595-598.e595. https://doi.org/10.1053/j.gastro.2014.06.009 (2014).
45. Zhang, Y. & Lu, H. Signaling to p53: Ribosomal proteins find their way. *Cancer Cell* **16**, 369–377. https://doi.org/10.1016/j.ccr.2009.09.024 (2009).
46. Ferreira-Cerca, S., Pöll, G., Gleizes, P. E., Tschochner, H. & Milkereit, P. Roles of eukaryotic ribosomal proteins in maturation and transport of pre-18S rRNA and ribosome function. *Mol. Cell* **20**, 263–275. https://doi.org/10.1016/j.molcel.2005.09.005 (2005).
47. Krishnan, R., Boddapati, N. & Mahalingam, S. Interplay between human nucleolar GNL1 and RPS20 is critical to modulate cell proliferation. *Sci. Rep.* **8**, 11421. https://doi.org/10.1038/s41598-018-29802-y (2018).

Acknowledgements

The authors sincerely thank Liu Xiaoyun's team at Peking University School of Basic Medicine for their excellent technical assistance.

Author contributions

X.H., J.L., Z.H. and B.X.: Writing – review & editing, Writing – original draft, Methodology, Investigation, Data curation. J.Z. and M.Y.: data duration. X.W., Y.L. and X.L.: project administration and software. S.C.: writ-

ing-original draft and formal analysis. P.W.: funding acquisition, supervision and writing-review & edit. All the authors have read and approved the final manuscript.

Funding
This work was supported by grants from Beijing Nova Program (No. 20230484244), Peking University Clinical Scientist Training Program (No. BMU2023PYJH001), supported by "the Fundamental Research Funds for the Central Universities", the National Natural Science Foundation of China (No. 32370837); National High Level Hospital Clinical Research Funding (Scientific and Technological Achievements Transformation Incubation Guidance Fund Project of Peking University First Hospital) (No. 2023CX04).

Declarations

Competing interests
The authors declare no competing interests.

Additional information
Supplementary Information The online version contains supplementary material available at https://doi.org/10.1038/s41598-025-02268-5.

Correspondence and requests for materials should be addressed to S.C. or P.W.

Reprints and permissions information is available at www.nature.com/reprints.

Publisher's note Springer Nature remains neutral with regard to jurisdictional claims in published maps and institutional affiliations.